ACS APPLIED MATERIALS & INTERFACES

Research Article

www.acsami.org

Three-Dimensional, Fibrous Lithium Iron Phosphate Structures Deposited by Magnetron Sputtering

Aiko Bünting,* Sven Uhlenbruck, Doris Sebold, H. P. Buchkremer, and R. Vaßen

Institute of Energy and Climate Research, Materials Synthesis and Processing (IEK-1), Forschungszentrum Jülich GmbH, 52425 Jülich, Germany

Supporting Information

ABSTRACT: Crystalline, three-dimensional (3D) structured lithium iron phosphate ($LiFePO_4$) thin films with additional carbon are fabricated by a radio frequency (RF) magnetron-sputtering process in a single step. The 3D structured thin films are obtained at deposition temperatures of 600 °C and deposition times longer than 60 min by using a conventional sputtering setup. In contrast to glancing angle deposition (GLAD) techniques, no tilting of the substrate is required. Thin films are characterized by X-ray diffraction (XRD), Raman spectrospcopy, scanning electron microscopy (SEM), cyclic voltammetry (CV), and galvanostatic charging and discharging. The structured $LiFePO_4$ + C thin films consist of fibers that grow perpendicular to the substrate surface. The fibers have diameters up to 500 nm and crystallize in the desired olivine structure. The 3D structured thin films have superior electrochemical properties compared with dense two-dimensional (2D) $LiFePO_4$ thin films and are, hence, very promising for application in 3D microbatteries.

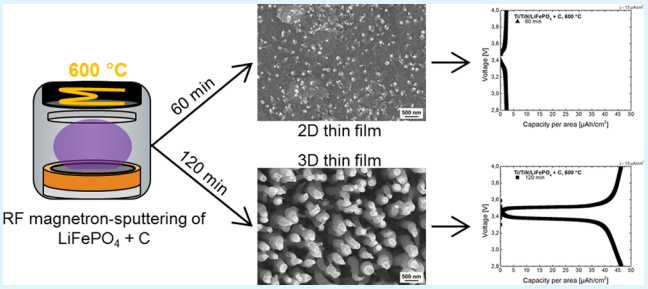

KEYWORDS: *3D microbattery, lithium iron phosphate, magnetron sputtering, nanostructured electrodes, lithium-ion battery, fibrous structures*

1. INTRODUCTION

$LiFePO_4$ was introduced as a low-cost cathode material for lithium-ion batteries by Padhi et al. in 1997. It is an environmentally benign, nontoxic material with a flat discharge plateau at 3.4 V vs Li, a high specific capacity of 170 mAh/g, and superior safety properties.[1,2] However, because of a low Li diffusivity and a low electronic conductivity, only a limited utilization can be achieved for pristine $LiFePO_4$.[3]

By coating $LiFePO_4$ with carbon, a utilization close to the theoretical value can be obtained.[4,5] The carbon coating has mainly three impacts: it enhances electronic conductivity,[6] avoids formation of trivalent iron impurities,[7] and reduces particle sizes.[8,9] In particular, a small particle size in the nanometer scale is an important factor to achieve high specific capacities.[10]

Nanostructured electrode materials are in general very promising for application in lithium-ion batteries as discussed in several reviews.[11−15] They offer a short lithium-ion transport distance and a high contact area to the electrolyte, which increases the number of sites for the lithium-ion transfer. Consequently, the rate capability can be enhanced and polarization losses can be reduced. Furthermore, nanostructured electrode materials have a high tolerance toward volume expansions that occur during intercalation and deintercalation processes.

Nanostructured materials can be fabricated by a variety of methods. Solution-based methods like sol−gel, solvothermal, microemulsion, or electrochemical deposition but also chemical and physical vapor deposition (CVD/PVD) are used for the fabrication of nanostructured materials.[11,16] Among these methods, techniques that allow the growth of nanostructured electrodes directly on current collectors are very promising because no electrode slurry has to be fabricated and casted. Furthermore, the addition of electrode additives like binders is not necessary, which increases the gravimetric capacity of the battery. Electrodes that are directly grown on current collectors are called "self-supported" electrodes.[13]

Self-supported electrodes can be obtained by PVD.[17] For obtaining 3D structured electrodes by PVD, in general, a special technique called oblique or glancing angle deposition (OAD or GLAD) has to be used.[18−20] During GLAD the substrate is inclined toward the deposition source, which is why the material arrives at the substrate under an oblique angle. Because of shadowing effects, micro- and nanostructured thin films are obtained.[21−23] Because of the oblique angle, however, lower deposition rates compared to the ones of conventional experimental setups are obtained.[24]

In this article synthesis and characterization of self-supported 3D structured $LiFePO_4$ electrodes with additional carbon ($LiFePO_4$ + C) by physical vapor deposition (PVD) are

Received: August 2, 2015
Accepted: September 18, 2015
Published: September 18, 2015

DOI: 10.1021/acsami.5b07090
ACS Appl. Mater. Interfaces 2015, 7, 22594−22600

presented. For the first time, 3D structured $LiFePO_4$ + C thin films were successfully deposited by a simple RF magnetron sputtering process using a conventional setup and a type-2 unbalanced magnetron as described by Kelly and Arnell.[25] No tilting of the substrate and, thus, no GLAD setup is necessary to grow the structured $LiFePO_4$ + C electrode.

Moreover, no template or catalyst is used for the fabrication, which is why ready-to-use 3D structured $LiFePO_4$ + C thin films can be synthesized in a single step without any pre- or postprocessing. In addition, the fabrication of 3D structures by magnetron sputtering offers the advantages of avoiding any toxic precursors and the ability to scale up the process to large substrates.

The 3D $LiFePO_4$ + C thin films were deposited on titanium nitride (TiN)-coated titanium (Ti) foils. The resulting 3D thin films exhibit superior electrochemical performances and are very promising for application in 3D microbatteries.[13,21,26−28]

2. EXPERIMENTAL SECTION

2.1. $LiFePO_4$ + C Thin-Film Preparation. TiN-coated Ti foils were used as substrates. The fabrication of the TiN coating is reported elsewhere.[29] The substrates were cleaned with ethanol in an ultrasonic bath for 15 min and by a sputter-etching process immediately before the deposition of $LiFePO_4$ + C. After sputter-etching, the substrates were transferred to the sputtering chamber without breaking the vacuum.

For the sputtering process, a commercial $LiFePO_4$ target with 7 m% carbon (EVOCHEM Advanced Materials GmbH, Germany) and a diameter of 249 mm was used. The base pressure of the sputtering chamber was kept at 10^{-8} mbar. Prior to each deposition the target surface was cleaned by sputtering with a closed shutter for 10 min.

The $LiFePO_4$ + C thin films were deposited by an unbalanced RF magnetron sputtering process in pure Argon at a gas flow of 20 sccm. During deposition the argon was kept at a pressure of 5×10^{-3} mbar and a power of 600 W (1.2 W/cm^2) was applied. The depositions were conducted at room temperature, 400, 500, and 600 °C and lasted for 60, 120, and 240 min. After the depositions at elevated temperatures, the samples were cooled down to room temperature with a cooling rate of nominally 5 K/min.

The deposition rate was $3.1 \pm 0.2 \times 10^{-4}$ g/(cm^2 h). It was determined at room temperature (RT) by depositing $LiFePO_4$ + C on an area of 24 cm^2 for 7.25 and 8.5 h. For this experiment, borosilicate glass substrates, which were weighed before and after the deposition, were used instead of TiN-coated Ti foils. The obtained weight gain was divided by the area and the deposition time to estimate the deposition rate. For the balancing, a M Power balance (Sartorius Weighing Technology GmbH, Germany) with a readability of 0.1 mg was used.

2.2. Characterization. The crystal structures of the thin films were analyzed by a Bruker D4 Endeavor (Bruker AXS GmbH, Germany) using Cu Kα radiation. Microstructure characterization was done by a Zeiss Ultra 55 SEM (Carl Zeiss NTS GmbH, Germany). For the Raman spectroscopy an argon ion laser with an excitation wavelength of 488 nm (Coherent Ltd., U.S.A.), a Jobin iHR320 spectrometer (HORIBA Scientific, U.S.A.), and a IDus 420 charge-coupled device (CCD) camera (Andor Technology Ltd., U.K.) were used. The electrochemical performance was measured versus metallic lithium (Li) in a two-electrode setup using EL-cells (EL-cell GmbH, Germany). $LiPF_6$ (1 M) in a mixture of ethylene carbonate (EC) and dimethyl carbonate (DMC) in 1:1 volume ratio was used as electrolyte. Cyclic voltammetry was performed between 2.8 and 4.0 V at a scan rate of 1 mV/s. Galvanostatic charging and discharging were also done between 2.8 and 4.0 V. For the electrochemical characterization a Biologic VMP-300 multipotentiostat (BioLogic Science Instruments, France) was used.

3. RESULTS AND DISCUSSION

The XRD patterns of $LiFePO_4$ + C thin films deposited at RT, 400, 500, and 600 °C for 240 min are shown in Figure 1. A

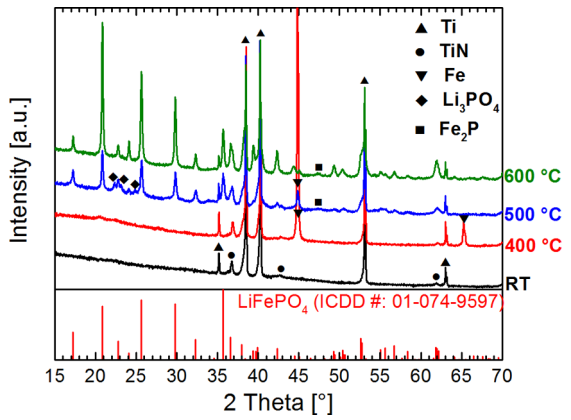

Figure 1. XRD patterns of $LiFePO_4$ + C thin films deposited for 240 min at RT, 400, 500, and 600 °C. Below the measured XRD patterns, $LiFePO_4$ reference positions and intensity ratios are shown.

crystalline $LiFePO_4$ structure can be observed at 500 and 600 °C. At 600 °C the $LiFePO_4$ reflections peaks are more intense, which indicates an enhanced crystal structure. All depicted thin films are expected to have the same $LiFePO_4$ mass because they all have been deposited for the same period of time (240 min).

The thin film deposited at RT is amorphous, and only reflection peaks from the Ti substrate and TiN are visible. At a deposition temperature of 400 °C, the thin film exhibits two reflection peaks at $2\theta \approx 45°$ and $2\theta \approx 65°$. The reflection peak at $2\theta \approx 45°$ is also observable at 500 °C, even though it has a much lower intensity. Due to the much lower intensity, the corresponding and weaker reflection peak at $2\theta \approx 65°$ is probably superimposed by background radiation. The reflection peaks at $2\theta \approx 45°$ and $2\theta \approx 65°$ can be assigned to metallic iron. The formation of metallic iron in conjunction with the deposition of $LiFePO_4$ thin films has been reported a few times.[29−31] However, in those cases $LiFePO_4$ was deposited without carbon and the formation of iron was attributed to an interdiffusion between the substrate and the deposited $LiFePO_4$. For the samples discussed in this article, a TiN interlayer is used, which effectively blocks interdiffusion.[29] Therefore, it is more likely that the formation of metallic iron results from a reduction by the present carbon (carbothermal reduction).

The occurrence of a carbothermal reduction is further supported by lithium phosphate (Li_3PO_4) and iron phosphide (Fe_2P) impurity phases, which probably cause weak reflection peaks in the pattern of the sample deposited at 500 °C. The formation of Li_3PO_4 and Fe_2P impurity phases is explained by a carbothermal reduction of $LiFePO_4$[32,33] as described by eq 1:[34]

$$6LiFePO_4 + 8C \rightarrow 3Fe_2P + 2Li_3PO_4 + 8CO_2 \uparrow + P\uparrow \quad (1)$$

The weak Fe_2P reflection peak is also detected in the XRD pattern of the sample deposited at 600 °C, which indicates that the carbothermal reduction of $LiFePO_4$ also occurs at this temperature. The reflection peaks of metallic iron are not visible at 600 °C.

According to this observations, we assume that the products of the carbothermal reduction depend on the structure of the

DOI: 10.1021/acsami.5b07090
ACS Appl. Mater. Interfaces 2015, 7, 22594−22600

$LiFePO_4$ thin film. In the case of amorphous $LiFePO_4$ thin films (400 °C), the carbothermal reduction leads to the formation of metallic iron, and in case of crystalline $LiFePO_4$ thin films (600 °C), the carbothermal reduction leads to the formation of Fe_2P. At 500 °C the $LiFePO_4$ thin film is partially amorphous as well as crystalline, and thus, iron as well as Fe_2P develop.

Because of the fact that crystalline $LiFePO_4$ thin films possess superior electrochemical properties,[35] the rest of the article focuses on $LiFePO_4$ + C thin films deposited at 500 and 600 °C. For further information on Raman spectra and SEM images of thin films deposited at RT and 400 °C, see the Supporting Information.

Raman spectra were measured to confirm the presence of graphite in $LiFePO_4$ + C thin films deposited at 500 and 600 °C and are shown in Figure 2. Both spectra exhibit peaks at

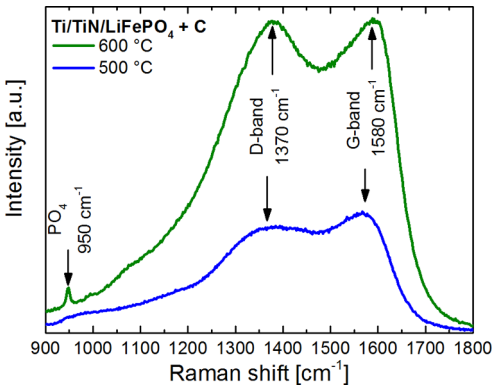

Figure 2. Raman spectra of $LiFePO_4$ + C thin films deposited at 500 and 600 °C for 240 min.

around 1370 and 1580 cm^{-1}, which are characteristic for graphite.[36−38] The peaks at 1370 and at 1580 cm^{-1} can be assigned to disordered graphite and to crystalline graphite, respectively.[39]

In contrast to the spectrum of the sample deposited at 500 °C, a peak at 950 cm^{-1} is visible at 600 °C. This peak can be assigned to a vibration of the PO_4 group.[36−38] This observation further underpins an enhanced crystal structure compared with the $LiFePO_4$ + C thin film deposited at 500 °C.

The morphology of the samples deposited at 500 and 600 °C is characterized by SEM. Secondary electron images of the surface are shown in Figure 3a−d. The morphology of the resulting thin film strongly depends on the deposition temperature. At 500 °C a single crack and a waved surface are visible at lower magnification (Figure 3a). To some extent, the waved structure can be traced back to scratches (indexed by red arrows) in the Ti substrate. At higher magnification (Figure 3b) a dense structure and slightly waved surface of the thin film becomes apparent.

At a deposition temperature of 600 °C, the morphology of the thin film has completely changed. At lower magnification (Figure 3c), bright and dark areas are visible that indicate a rough surface. The higher magnification (Figure 3d) reveals the detailed structure of the thin film. The bright areas can be assigned to tips of fibers, which have grown perpendicular to the surface of the substrate. The dark areas correspond to the space between the fibers. The fibers have a diameter up to ~500 nm that decreases with increasing height. Because of multiple tips, it seems as if the fibers consist of multiple single

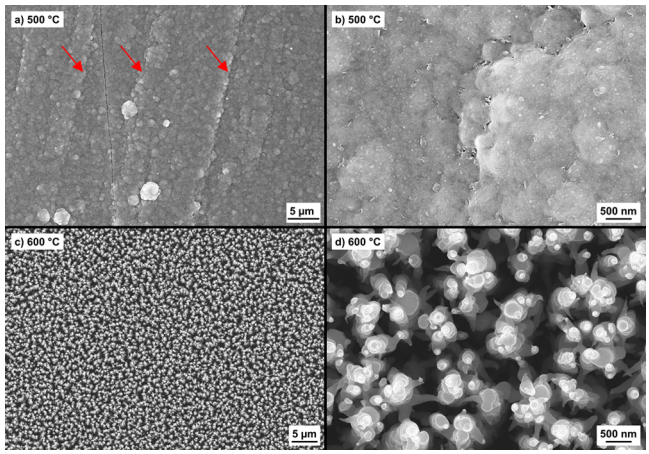

Figure 3. SEM surface images of the samples deposited for 240 min at 500 °C (a, b) and at 600 °C (c, d). On the left side (a, c) images at lower magnification are shown, and on the right side (b, d) images at higher magnification are shown. The red arrows indicate scratches originating from the Ti foil.

fibers that have merged together during the growth process. Due to the fiber structure the total surface area of the thin film has increased compared with dense 2D thin films.

CV measurements were conducted to prove the electrochemical activity of the thin films and are shown in Figure 4.

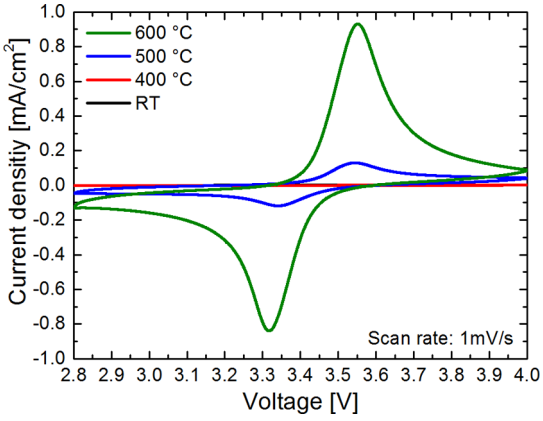

Figure 4. CV results of the thin films deposited for 240 min at RT, 400, 500, and 600 °C.

Thin films deposited at RT and 400 °C do not exhibit the typical redox couple of $LiFePO_4$ at ~3.5 V, which can be explained by the amorphous structure of the $LiFePO_4$ thin film resulting in a low electrochemical activity.[35]

Thin films deposited at 500 and 600 °C with a crystalline $LiFePO_4$ structure exhibit the desired redox couple of $LiFePO_4$ at ~3.5 V. However, the redox couple of the sample deposited at 600 °C has much higher peak currents, which indicates a much higher capacity and, hence, a much better electrochemical performance.

The much higher extractable capacity for the thin film deposited at 600 °C is confirmed by galvanostatic charging and discharging at a current density of ~10 $\mu A/cm^2$ (0.05 C). The resulting charge and discharge curves are shown in Figure 5. The samples deposited at 500 and 600 °C have capacities per area of around 20 and 120 $\mu Ah/cm^2$, respectively. This is nearly a 6-fold increase in capacity at constant electrode masses. The

DOI: 10.1021/acsami.5b07090
ACS Appl. Mater. Interfaces 2015, 7, 22594−22600

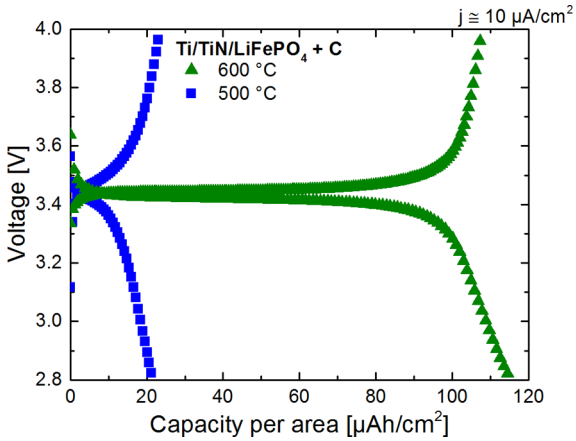

Figure 5. Galvanostatic charging and discharging at a current density of 10 μA/cm^2 for the samples deposited at 500 and 600 °C for 240 min.

increase can be explained by the enhanced crystallinity and the higher specific surface area for the thin film deposited at 600 °C.

The $LiFePO_4$ + C thin film deposited at 600 °C has a very high capacity per area compared with dense $LiFePO_4$ thin films. A capacity per area of ∼10 μAh/cm^2 was reported for a dense, 320 nm thick $LiFePO_4$ thin film.[40] Even a 1.5 μm thick $LiFePO_4$ thin film only achieved a capacity density of ∼38 μAh/(cm^2 μm), which is equal to capacity per area of ∼60 μAh/cm^2.[41]

The cycling behavior at different C-rates of the thin film deposited at 600 °C is shown in Figure 6. The sample possesses

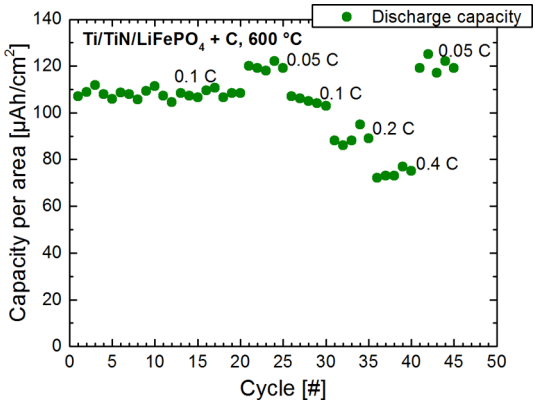

Figure 6. Discharge capacity as a function of the cycle number at different C-rates for the sample deposited at 600 °C for 240 min. The sample was charged and discharged between 2.8 and 4.0 V.

a stable discharge capacity over at least 45 cycles. However, in comparison with a 3D structured $LiFePO_4$ electrode made by a more complex template method,[42] the rate capability is still improvable. By increasing the C-rate from 0.1 to 0.4 C, the extractable discharge capacity decreases from ∼110 to ∼70 μAh/cm^2, which is equal to a capacity loss of ∼40%.

3.1. Characterization of Samples Deposited for 60 and 120 min. Thin films have been deposited for 60 and 120 min at 600 °C to characterize the influence of the deposition time on the resulting morphology and electrochemical performance. The XRD patterns and Raman spectra of thin films deposited for 60 and 120 min are shown in Figure 7a and b, respectively. Beside $LiFePO_4$ reflection peaks, both XRD patterns exhibit Fe_2P and Li_3PO_4 impurity phases that can be related to the carbothermal reduction of $LiFePO_4$ (see eq 1). The less intense reflection peaks of the thin film deposited for 60 min can be explained by a lower $LiFePO_4$ mass due to the shorter deposition time.

The Raman spectra of the thin films deposited for 60 and 120 min exhibit the characteristic D-band and G-band, which can be assigned to disordered and crystalline graphite, respectively. In both spectra a peak at 950 cm^{-1} is visible that can be assigned to the PO_4 group and that indicates an enhanced crystallinity. Consequently, the XRD patterns as well as the Raman spectra resemble the ones for the thin film deposited at 600 °C for 240 min.

SEM images of the samples deposited for 60 and 120 min at 600 °C are shown in Figure 8. The images reveal that the 3D structure does not directly start to grow from the beginning of the deposition. After a deposition time of 60 min, the surface of the sample is still flat. At lower magnification (Figure 8a), some globular structures are visible at the surface (indexed by arrows). At higher magnification (Figure 8b), a slightly structured surface and some small cracks are apparent. However, no fibers can be observed and, thus, the specific surface area of this sample is not significantly increased.

On the other hand, the thin film deposited for 120 min possesses a 3D structure. At lower magnification (Figure 8c), brighter and darker areas are visible. At higher magnification (Figure 8d), the brighter areas can be attributed to the tips of the fibers while the darker areas can be attributed to the space between the fibers. Compared with the fibers grown for 240 min in Figure 3d, the fibers are less merged and have, thus, an average diameter of <500 nm.

The galvonstatic charge and discharge curves of the samples deposited at 600 °C for 60 and 120 min are shown in Figure 9. The samples were charged and discharged at a current density of 13 μA/cm^2, which is equal to a C-rate of 0.3 C (60 min) and 0.15 C (120 min).

The sample deposited for 120 min offers a nearly 20 times higher capacity per area than the sample deposited for 60 min. Because the XRD and Raman results have shown that both thin films have a comparable crystal structure and contain graphite, the increase in capacity is mainly attributed to the emergence of the fiber structure and the related increase in surface area.

The extractable capacity per area as a function of the deposition time is shown in Figure 10. The theoretical capacity is displayed by a dashed line and estimated by the mass deposition rate (0.3 mg/(cm^2 h), see Experimental Section) multiplied with the specific capacity of $LiFePO_4$ (170 mAh/g). Taking into account that up to 7 mass% are inactive carbon, a capacity deposition rate of ∼50 μAh/(cm^2 h) is obtained.

The flat thin film has only a very low utilization of ∼5%. Such a low utilization has been reported several times for $LiFePO_4$ thin films and is mainly attributed to the low ionic conductivity of $LiFePO_4$.[29,43,44]

For the 3D structured thin film the capacity per area increases. Related to the theoretical capacity of the entire thin film, a utilization of ∼50% (≈85 mAh/g) is achieved for the thin films (120 and 240 min). The utilization only of the 3D structured part can be estimated by shifting the inset of the theoretical capacity by 1 h (depicted by the solid black line). By this, we neglect the contribution of the 2D thin film, which grows during the first hour of deposition, to the total capacity. By comparing the capacity per area with the values given by the

DOI: 10.1021/acsami.5b07090
ACS Appl. Mater. Interfaces 2015, 7, 22594−22600

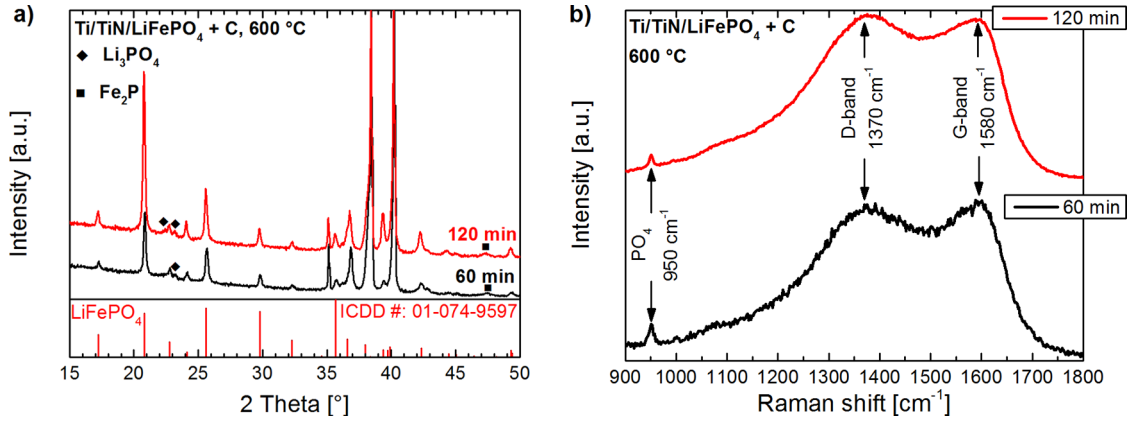

Figure 7. XRD patterns (a) and Raman spectra (b) of the thin films deposited at 600 °C for 60 and 120 min.

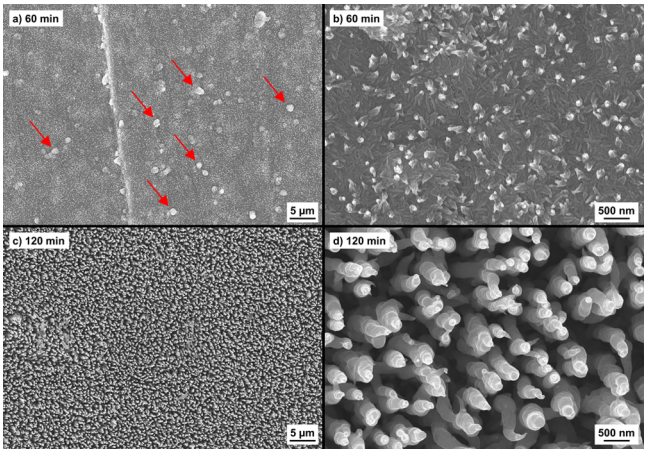

Figure 8. SEM images of the samples deposited at 600 °C for 60 min (a, b) and 120 min (c, d). On the left side (a, c) images at lower magnification are shown, and on the right side (b, d) images at higher magnification are shown.

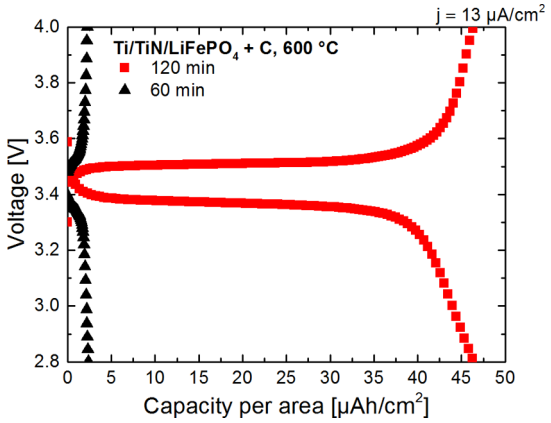

Figure 9. Galvanostatic charging and discharging of the samples deposited at 600 °C for 60 and 120 min between 2.8 and 4.0 V at a current density of ~13 μA/cm^2.

black solid line, the thin films deposited for 120 and 240 min achieve a utilization of ~95% (≈160 mAh/g at 0.15 C) and 80% (≈135 mAh/g at 0.05 C), respectively. The higher utilization at a higher C-rate for the thin film deposited for 120 min can be explained by the smaller fiber diameter and, thus, shorter diffusion length.

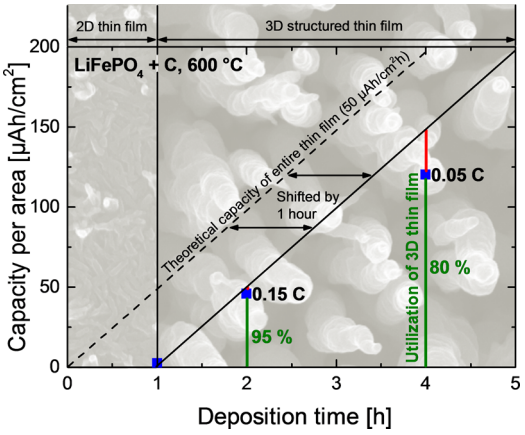

Figure 10. Capacity per area as a function of the deposition time. The theoretical capacity as a function of the deposition time is depicted by the dashed line. See text for further information.

Figure 10 shows that a high utilization and, thus, specific capacity of the 3D structured part of the $LiFePO_4$ thin film can be achieved. In comparison with the published specific capacities of plane $LiFePO_4$ thin films made by magnetron sputtering,[45−47] these specific capacities are among the highest. However, there are still challenges remaining. The 3D structure should evolve right from the beginning of the deposition to increase the overall utilization. In addition, fibers with a small diameter are promising for high rate capabilities, which is why a merging of fibers with prolonged deposition time should be avoided.

3.2. Formation of 3D Structure. The formation of a 3D structured $LiFePO_4$ + C thin film by conventional magnetron sputtering at high deposition temperatures is unexpected. According to structure zone models (SZM) proposed by Movchan and Demchishin and further developed by Thornton, porous thin films can be obtained at low deposition temperatures. By increasing the deposition temperature, denser thin film structures are expected due to higher surface diffusion.[48−50]

Exceptions from this behavior were reported for metals like nickel, gold, silver, and aluminum.[51] Jankowski and Hayes observed that these metals form porous thin films at elevated temperatures of ~0.5T_{melt} (substrate temperature normalized to the absolute melting point T_{melt} of the deposited material) and at pressures between 5 and 15 mTorr (≈6.5 × 10^{-3} to 2 × 10^{-2} mbar). The formation of the porous metal structures was

DOI: 10.1021/acsami.5b07090
ACS Appl. Mater. Interfaces 2015, 7, 22594−22600

related to a high surface diffusion and the onset of recrystallization processes leading to grain growth oblique to the substrate surface. Accordingly, Jankowski and Hayes suggested to add a further zone (Zone S) to the SZM for metals. A similar behavior was also observed for zinc.[52]

Another exception was reported for boron.[53] Well-aligned amorphous boron nanowire arrays were obtained at deposition temperatures of 800 °C by a simple RF magnetron sputtering process. At lower deposition temperatures a continuous film was obtained. In this case the growth of the nanowires was explained by a vapor-cluster-solid mechanism.[54]

In summary, reports on the formation of 3D structures at elevated temperatures by a simple magnetron sputtering process can be found. However, to our knowledge such 3D structures were only observed for pure elements like metals or boron (containing only a small amount of oxygen) and not for compounds like $LiFePO_4$. Different mechanisms are used to explain the formation of porous metal structures and boron nanowires. Because the deposition temperature of the $LiFePO_4$ + C thin films is rather high (~0.7T_{melt}, T_{melt} of $LiFePO_4$ is ~1000 °C[55]), recrystallization processes, like those expected for the formation of porous metals, could play a role. However, further experiments are needed to clarify the growth process of the self-organized 3D structured $LiFePO_4$ + C thin films in detail.

4. CONCLUSION

3D structured $LiFePO_4$ + C thin films have been fabricated by a simple magnetron sputtering process in a single step without any pre- or postprocessing. The 3D structures are obtained at elevated temperatures (600 °C) and prolonged deposition times (>60 min). The 3D structured $LiFePO_4$ + C thin films consist of fibers with a diameter of up to 500 nm that grow perpendicular to the substrate surface. The 3D $LiFePO_4$ + C thin films have the desired crystal structure and show superior electrochemical properties compared with 2D thin films. Therefore, they are very promising for application in 3D microbatteries.

A reduction of the fiber diameter and an onset of the fiber growth right from the beginning of the deposition are desired to further increase the electrochemical performance. A detailed understanding of the growth mechanism is important to achieve these goals. This needs further experiments and will be the topic of an upcoming paper.

■ ASSOCIATED CONTENT

Supporting Information

The Supporting Information is available free of charge on the ACS Publications website at DOI: 10.1021/acsami.5b07090.

SEM images and Raman spectra of $LiFePO_4$ + C thin films deposited at RT and 400 °C (PDF)

■ AUTHOR INFORMATION

Corresponding Author

*E-mail: a.buenting@fz-juelich.de. Phone: +492461612877. Fax: +492461612455.

Notes

The authors declare no competing financial interest.

■ ACKNOWLEDGMENTS

The authors thank Marcus Hülsbeck from IEK-5 for performing Raman measurements. Financial support by Helmholtz Gemeinschaft Deutscher Forschungszentren e.V. under Grants "Elektrochemische Speicher im System - Zuverlässigkeit und Integration" and "Helmholtz-Initiative für Mobile/Stationäre Energiespeichersysteme" are gratefully acknowledged.

■ REFERENCES

(1) Padhi, A. K.; Nanjundaswamy, K. S.; Goodenough, J. B. Phospho-Olivines as Positive-Electrode Materials for Rechargeable Lithium Batteries. *J. Electrochem. Soc.* **1997**, *144*, 1188−1194.

(2) Yamada, A.; Chung, S. C.; Hinokuma, K. Optimized $LiFePO_4$ for Lithium Battery Cathodes. *J. Electrochem. Soc.* **2001**, *148*, A224−A229.

(3) Yuan, L.-X.; Wang, Z.-H.; Zhang, W.-X.; Hu, X.-L.; Chen, J.-T.; Huang, Y.-H.; Goodenough, J. B. Development and Challenges of $LiFePO_4$ Cathode Material for Lithium-Ion Batteries. *Energy Environ. Sci.* **2011**, *4*, 269−284.

(4) Ravet, N.; Chouinard, Y.; Magnan, J. F.; Besner, S.; Gauthier, M.; Armand, M. Electroactivity of Natural and Synthetic Triphylite. *J. Power Sources* **2001**, *97*−*98*, 503−507.

(5) Franger, S.; Le Cras, F.; Bourbon, C.; Rouault, H. LiFePO4 Synthesis Routes for Enhanced Electrochemical Performance. *Electrochem. Solid-State Lett.* **2002**, *5*, A231−A233.

(6) Hu, Y. S.; Guo, Y. G.; Dominko, R.; Gaberscek, M.; Jamnik, J.; Maier, J. Improved Electrode Performance of Porous $LiFePO_4$ Using RuO_2 as an Oxidic Nanoscale Interconnect. *Adv. Mater.* **2007**, *19*, 1963−1966.

(7) Ait-Salah, A.; Zaghib, K.; Mauger, A.; Gendron, F.; Julien, C. M. Magnetic Studies of the Carbothermal Effect on $LiFePO_4$. *Phys. Status Solidi A* **2006**, *203*, R1−R3.

(8) Shin, H. C.; Cho, W. I.; Jang, H. Electrochemical Properties of the Carbon-Coated LiFePO(4) as a Cathode Material for Lithium-Ion Secondary Batteries. *J. Power Sources* **2006**, *159*, 1383−1388.

(9) Yun, N. J.; Ha, H. W.; Jeong, K. H.; Park, H. Y.; Kim, K. Synthesis and Electrochemical Properties of Olivine-Type $LiFePO_4$/C Composite Cathode Material Prepared from a Poly(vinyl alcohol)-Containing Precursor. *J. Power Sources* **2006**, *160*, 1361−1368.

(10) Gaberscek, M.; Dominko, R.; Jamnik, J. Is Small Particle Size More Important than Carbon Coating? An Example Study on $LiFePO_4$ Cathodes. *Electrochem. Commun.* **2007**, *9*, 2778−2783.

(11) Wang, Y.; Cao, G. Z. Developments in Nanostructured Cathode Materials for High-Performance Lithium-Ion Batteries. *Adv. Mater.* **2008**, *20*, 2251−2269.

(12) Song, M.-K.; Park, S.; Alamgir, F. M.; Cho, J.; Liu, M. Nanostructured Electrodes for Lithium-Ion and Lithium-Air Batteries: The Latest Developments, Challenges, and Perspectives. *Mater. Sci. Eng., R* **2011**, *72*, 203−252.

(13) Ellis, B. L.; Knauth, P.; Djenizian, T. Three-Dimensional Self-Supported Metal Oxides for Advanced Energy Storage. *Adv. Mater.* **2014**, *26*, 3368−3397.

(14) Roy, P.; Srivastava, S. K. Nanostructured Anode Materials for Lithium Ion Batteries. *J. Mater. Chem. A* **2015**, *3*, 2454−2484.

(15) Myung, S.-T.; Amine, K.; Sun, Y.-K. Nanostructured Cathode Materials for Rechargeable Lithium Batteries. *J. Power Sources* **2015**, *283*, 219−236.

(16) Tiwari, J. N.; Tiwari, R. N.; Kim, K. S. Zero-Dimensional, One-Dimensional, Two-Dimensional and Three-Dimensional Nanostructured Materials for Advanced Electrochemical Energy Devices. *Prog. Mater. Sci.* **2012**, *57*, 724−803.

(17) Teki, R.; Datta, M. K.; Krishnan, R.; Parker, T. C.; Lu, T. M.; Kumta, P. N.; Koratkar, N. Nanostructured Silicon Anodes for Lithium Ion Rechargeable Batteries. *Small* **2009**, *5*, 2236−2242.

(18) Robbie, K.; Friedrich, L. J.; Dew, S. K.; Smy, T.; Brett, M. J. Fabrication of Thin Films with Highly Porous Microstructures. *J. Vac. Sci. Technol., A* **1995**, *13*, 1032−1035.

(19) Robbie, K.; Brett, M. J. Sculptured Thin Films and Glancing Angle Deposition: Growth Mechanics and Applications. *J. Vac. Sci. Technol., A* **1997**, *15*, 1460−1465.

DOI: 10.1021/acsami.5b07090
ACS Appl. Mater. Interfaces 2015, 7, 22594−22600

(20) Sit, J. C.; Vick, D.; Robbie, K.; Brett, M. J. Thin Film Microstructure Control Using Glancing Angle Deposition by Sputtering. *J. Mater. Res.* **1999**, *14*, 1197−1199.
(21) Fleischauer, M. D.; Li, J.; Brett, M. J. Columnar Thin Films for Three-Dimensional Microbatteries. *J. Electrochem. Soc.* **2009**, *156*, A33−A36.
(22) Horprathum, M.; et al. Ultrasensitive Hydrogen Sensor Based on Pt-Decorated WO_3 Nanorods Prepared by Glancing-Angle dc Magnetron Sputtering. *ACS Appl. Mater. Interfaces* **2014**, *6*, 22051−22060.
(23) Khare, C.; Stepanovich, A.; Buenconsejo, P. J. S.; Ludwig, A. Synthesis of WO_3 Nanoblades by the Dealloying of Glancing Angle Deposited W-Fe Nanocolumnar Thin Films. *Nanotechnology* **2014**, *25*, 205606.
(24) Manova, D.; Gerlach, J. W.; Mandl, S. Thin Film Deposition Using Energetic Ions. *Materials* **2010**, *3*, 4109−4141.
(25) Kelly, P. J.; Arnell, R. D. Magnetron Sputtering: A Review of Recent Developments and Applications. *Vacuum* **2000**, *56*, 159−172.
(26) Long, J. W.; Dunn, B.; Rolison, D. R.; White, H. S. Three-Dimensional Battery Architectures. *Chem. Rev.* **2004**, *104*, 4463−4492.
(27) Oudenhoven, J. F. M.; Baggetto, L.; Notten, P. H. L. All-Solid-State Lithium-Ion Microbatteries: A Review of Various Three-Dimensional Concepts. *Adv. Energy Mater.* **2011**, *1*, 10−33.
(28) Roberts, M.; et al. 3D Lithium Ion Batteries—From Fundamentals to Fabrication. *J. Mater. Chem.* **2011**, *21*, 9876−9890.
(29) Bünting, A.; Uhlenbruck, S.; Dellen, C.; Finsterbusch, M.; Tsai, C. L.; Sebold, D.; Buchkremer, H. P.; Vaßen, R. Influence of Titanium Nitride Interlayer on the Morphology, Structure and Electrochemical Performance of Magnetron-Sputtered Lithium Iron Phosphate Thin Films. *J. Power Sources* **2015**, *281*, 326−333.
(30) Legrand, C.; Dupont, L.; Tang, K.; Li, H.; Huang, X. J.; Baudrin, E. Structural and Textural Characterization of $LiFePO_4$ Thin Films Prepared by Pulsed Laser Deposition on Si Substrates. *Thin Solid Films* **2010**, *518*, 5447−5451.
(31) Legrand, C.; Dupont, L.; Davoisne, C.; le Marrec, F.; Perriere, J.; Baudrin, E. Unexpected Formation by Pulsed Laser Deposition of Nanostructured Fe/Olivine Thin Films on MgO Substrates. *J. Solid State Chem.* **2011**, *184*, 351−356.
(32) Arnold, G.; Garche, J.; Hemmer, R.; Strobele, S.; Vogler, C.; Wohlfahrt-Mehrens, A. Fine-Particle Lithium Iron Phosphate $LiFePO_4$ Synthesized by a New Low-Cost Aqueous Precipitation Technique. *J. Power Sources* **2003**, *119-121*, 247−251.
(33) Herle, P. S.; Ellis, B.; Coombs, N.; Nazar, L. F. Nano-Network Electronic Conduction in Iron and Nickel Olivine Phosphates. *Nat. Mater.* **2004**, *3*, 147−152.
(34) Rho, Y. H.; Nazar, L. F.; Perry, L.; Ryan, D. Surface Chemistry of $LiFePO_4$ Studied by Mossbauer and X-ray Photoelectron Spectroscopy and Its Effect on Electrochemical Properties. *J. Electrochem. Soc.* **2007**, *154*, A283−A289.
(35) Zhu, X.-J.; Cheng, L.-B.; Wang, C.-G.; Guo, Z.-P.; Zhang, P.; Du, G.-D.; Liu, H.-K. Preparation and Characteristics of $LiFePO_4$ Thin Film by Radio Frequency Magnetron Sputtering for Lithium Microbatteries. *J. Phys. Chem. C* **2009**, *113*, 14518−14522.
(36) Song, S. W.; Reade, R. P.; Kostecki, R.; Striebel, K. A. Electrochemical Studies of the $LiFePO_4$ Thin Films Prepared with Pulsed Laser Deposition. *J. Electrochem. Soc.* **2006**, *153*, A12−A19.
(37) Lu, Z. G.; Cheng, H.; Lo, M. F.; Chung, C. Y. Pulsed Laser Deposition and Electrochemical Characterization of $LiFePO_4$-Ag Composite Thin Films. *Adv. Funct. Mater.* **2007**, *17*, 3885−3896.
(38) Hong, J.; Wang, C.; Dudney, N. J.; Lance, M. J. Characterization and Performance of $LiFePO_4$ Thin-Film Cathodes Prepared with Radio-Frequency Magnetron-Sputter Deposition. *J. Electrochem. Soc.* **2007**, *154*, A805−A809.
(39) Reich, S.; Thomsen, C. Raman Spectroscopy of Graphite. *Philos. Trans. R. Soc., A* **2004**, *362*, 2271−2288.
(40) Köhler, M.; Berkemeier, F.; Gallasch, T.; Schmitz, G. Lithium Diffusion in Sputter-Deposited Lithium Iron Phosphate Thin-Films. *J. Power Sources* **2013**, *236*, 61−67.
(41) Rosaiah, P.; Hussain, O. M. Microstructural and Electrochemical Properties of RF-Sputtered $LiFePO_4$ Thin Films. *Ionics* **2014**, *20*, 1095−1101.
(42) Liu, Y.; Zhang, W.; Zhu, Y.; Luo, Y.; Xu, Y.; Brown, A.; Culver, J. N.; Lundgren, C. A.; Xu, K.; Wang, Y.; Wang, C. Architecturing Hierarchical Function Layers on Self-Assembled Viral Templates as 3D Nano-Array Electrodes for Integrated Li-Ion Microbatteries. *Nano Lett.* **2013**, *13*, 293−300.
(43) Sauvage, F.; Baudrin, E.; Gengembre, L.; Tarascon, J. M. Effect of Texture on the Electrochemical Properties of $LiFePO_4$ Thin Films. *Solid State Ionics* **2005**, *176*, 1869−1876.
(44) Sauvage, F.; Baudrin, E.; Laffont, L.; Tarascon, J. M. Origin of Electrochemical Reactivity Enhancement of Post-Annealed $LiFePO_4$ Thin Films: Preparation of Heterosite-Type $FePO_4$. *Solid State Ionics* **2007**, *178*, 145−152.
(45) Chiu, K. F.; Chen, P. Y. Structural Evolution and Electrochemical Performance of $LiFePO_4$/C Thin Films Deposited by Ionized Magnetron Sputtering. *Surf. Coat. Technol.* **2008**, *203*, 872−875.
(46) Xie, J.; Imanishi, N.; Zhang, T.; Hirano, A.; Takeda, Y.; Yamamoto, O. Li-Ion Diffusion Kinetics in $LiFePO_4$ Thin Film Prepared by Radio Frequency Magnetron Sputtering. *Electrochim. Acta* **2009**, *54*, 4631−4637.
(47) Bajars, G.; Kucinskis, G.; Smits, J.; Kleperis, J. Physical and Electrochemical Properties of $LiFePO_4$/C Thin Films Deposited by Direct Current and Radiofrequency Magnetron Sputtering. *Solid State Ionics* **2011**, *188*, 156−159.
(48) Movchan, B. A.; Demchishin, A. V. Study of Structure and Properties of Thick Vacuum Condensates of Nickel, Titanium, Tungsten, Aluminium Oxide and Zirconium Dioxide. *Phys. Met. Metallogr. (Transl. of Fiz. Met. Metalloved.)* **1969**, *28*, 83−90.
(49) Thornton, J. A. Influence of Apparatus Geometry and Deposition Conditions on Structure and Topography of Thick Sputtered Coatings. *J. Vac. Sci. Technol.* **1974**, *11*, 666−670.
(50) Thornton, J. A. Influence of Substrate Temperature and Deposition Rate on Structure of Thick Sputtered Cu Coatings. *J. Vac. Sci. Technol.* **1975**, *12*, 830−835.
(51) Jankowski, A. F.; Hayes, J. P. Sputter Deposition of a Spongelike Morphology in Metal Coatings. *J. Vac. Sci. Technol., A* **2003**, *21*, 422−425.
(52) Gazia, R.; Chiodoni, A.; Bianco, S.; Lamberti, A.; Quaglio, M.; Sacco, A.; Tresso, E.; Mandracci, P.; Pirri, C. F. An Easy Method for the Room-Temperature Growth of Spongelike Nanostructured Zn Films as Initial Step for the Fabrication of Nanostructured ZnO. *Thin Solid Films* **2012**, *524*, 107−112.
(53) Cao, L. M.; Zhang, Z.; Sun, L. L.; Gao, C. X.; He, M.; Wang, Y. Q.; Li, Y. C.; Zhang, X. Y.; Li, G.; Zhang, J.; Wang, W. K. Well-Aligned Boron Nanowire Arrays. *Adv. Mater.* **2001**, *13*, 1701−1704.
(54) Wang, Y. Q.; Duan, X. F.; Cao, L. M.; Wang, W. K. One-Dimensional Growth Mechanism of Amorphous Boron Nanowires. *Chem. Phys. Lett.* **2002**, *359*, 273−277.
(55) Gauthier, M.; Michot, C.; Ravet, N.; Duchesneau, M.; Dufour, J.; Liang, G.; Wontcheu, J.; Gauthier, L.; MacNeil, D. D. Melt Casting $LiFePO_4$. *J. Electrochem. Soc.* **2010**, *157*, A453−A462.

DOI: 10.1021/acsami.5b07090
ACS Appl. Mater. Interfaces 2015, 7, 22594−22600